Process Modeling and In-Situ Monitoring of Photopolymerization for Exposure Controlled Projection Lithography

Jenny Wang

Spring 2020

Faculty Signatures:

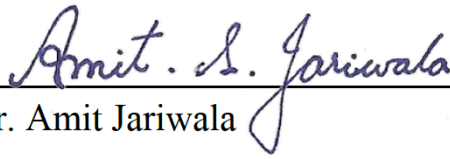

Dr. Amit Jariwala

Dr. David Rosen

TABLE OF CONTENTS

ABSTRACT

One of the main challenges in additive manufacturing is to ensure the consistent production of accurate and precise parts. Investigation of real-time monitoring and closed-loop feedback control for these processes is an area with great potential for discovery and innovation. These capabilities can vastly improve the quality and efficiency of production, and make additive manufacturing a lucrative option in a wide range of applications. Among the burgeoning field of additive manufacturing, stereolithography has proven to be an effective process to create a variety of products. However, the process lacks the resolution to manufacture small parts with a high degree of accuracy and precision. In order to meet the demand of modern technology, in which the use of micro-and nano-scale products is becoming more and more ubiquitous, a method of in-situ measurement and control for micro-stereolithography is being developed. Exposure controlled projection lithography (ECPL) is a micro-stereolithography process in which UV light is projected by a dynamic mask through a transparent substrate onto photopolymer resin to grow features from the substrate surface. The interferometric curing monitoring (ICM) system monitors the ECPL fabrication in real time, using the principles of interference optics to measure small changes in the dimensions of the cured part. Additionally, ECPL has been simulated using COMSOL software to characterize the reaction kinetics. The work presented in this thesis models the curing process based the simulation and based on information from the ICM system, and compares these results to develop a more complete understanding of the optical properties of ECPL. This could be used to establish a more accurate model to estimate the dimensions of the cured part in real time, which could then be used in a feedback-controlled system to fabricate more accurate and precise parts using ECPL.

1. INTRODUCTION

Photopolymerization is an additive manufacturing (AM) process that creates solid polymer structures by selectively shining light, often ultraviolet (UV) irradiation, onto a photosensitive monomer-rich bath. The work presented in this paper is based on Frontal Photopolymerization (FPP), which is characterized by the one-dimensional propagation of a planar curing front, or interface between the uncured liquid monomer and cured solid polymer, in the direction from which the light is exposed. [1] In ECPL, 3D features are cured in a photopolymer resin bath by UV light. The dimensions of the sample can be controlled by altering the curing radiation time and radiation profiles, which are prescribed by a series of bitmap images.

Recently, researchers such as Erdmann et al. [2] and Mizukami et al. [3] have developed similar techniques to the ECPL process. However, methods of controlling the process to achieve high accuracy and precision in the final cured shape were not presented. Jariwala et al. [4] subsequently developed a photopolymerization model to simulate the effects of oxygen inhibition during polymerization. Although modeling the oxygen inhibition process provided results that more closely matched the observed experimental trends, the model was found inadequate to predict the exact shape of the cured part.

This paper presents a more accurate, experimentally validated model with revised photopolymerization rate constants. Additionally, an integrated measurement method, the ICM system, has been implemented, using the principles of interference optics to monitor the dimensions of the cured part in real time. Results from the simulation and from ICM were

compared to verify the process model and gain a better understanding of the optical properties of the cured parts resulting from the ECPL process.

2. METHODS

This section outlines the methods and materials used in the study. Current experimental setups are presented, as well as the theoretical model of the ECPL process. Additionally, a real-time monitoring method for ECPL is introduced.

2.1. ECPL System

Figure 1 shows a schematic of the ECPL system. UV light is shined through the beam conditioning system, which homogenizes its intensity, onto the Digital Micromirror Device (DMD). The DMD is an array of square mirrors that can be oriented to display the desired pattern as prescribed by the image input, with each mirror corresponding to a pixel. The light is then reflected through the projection system, which resizes and focuses the image, and projects it into the resin chamber, where the part is cured. The resin chamber consists of liquid resin between two glass slides.

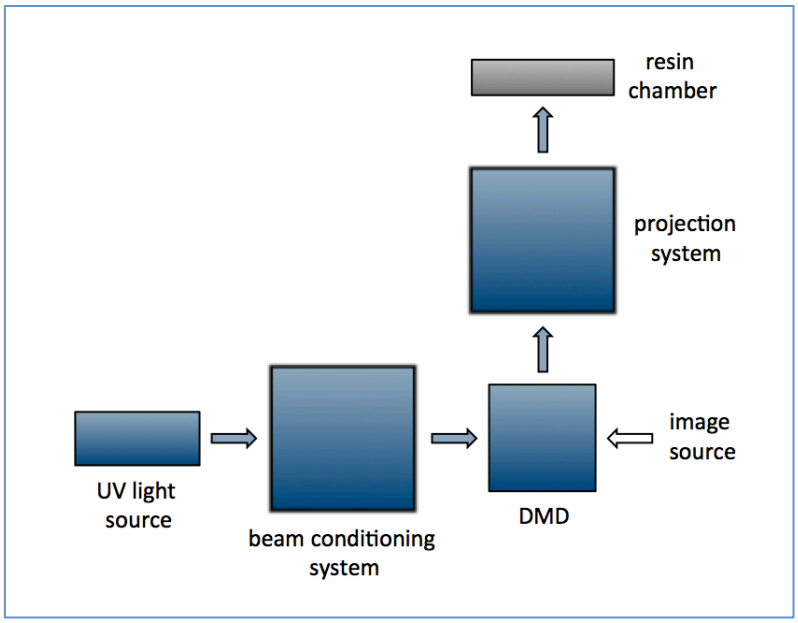

Figure 1: *Schematic of ECPL System*

2.2. ECPL process model

A COMSOL simulation of the ECPL process has been developed to predict the geometry of the cured part based on the sequence of curing radiation patterns and the time period of the exposure. This simulation models the photopolyermization reaction kinetics of the ECPL process.

2.2.1. Photopolymerization Model

Photopolymerization is the reaction of monomers or macromers to produce solid polymeric structures by light-induced initiation and polymerization [5]. The ECPL process uses acrylate monomers to fabricate the desired features. The resin consists of a 4:1 mass ratio of monomer and photoinitiator. The monomer is trimethylolpropane triacrylate (TMPTA) from Sartomer SR351h, and the photoinitiator is 2, 2-dimethoxy-1, 2-diphenylethan- 1-one (DMPA, IRGACURE-651) obtained from Ciba Specialty Chemicals. In stereolithography, a free radical is generated photo-chemically. The source of the photo-chemically generated radical is a photoinitiator molecule, which reacts with an actinic photon. This produces radicals that initiate the polymerization process.

To estimate the initiation rate constant, the light penetration depth is considered. According to Beer-Lambert's law of absorption, the light exposure at a depth z can be calculated using the Equation 1, where E_{max} is the exposure at the surface where $z = 0$, and D_p is the resin penetration depth at the given wavelength [6].

$$E(z) = E_{max} e^{-\frac{z}{D_p}} \tag{1}$$

The cure depth can be obtained using Equation 2, where E_c is the critical energy, the minimum exposure energy at which the resin will cure [6].

$$z = D_p ln\left(\frac{E}{E_c}\right) \tag{2}$$

However, Equations 1 and 2 assume that the attenuation of radiation through a cured layer and through the uncured resin is the same. Limaye and Rosen have determined that the attenuation through the cured material is significantly less than it is through the uncured resin [7]. Thus, Equation 2 is modified to Equation 3, where D_{pL} is the penetration depth in a liquid and D_{pS} is the penetration depth in a solid [5].

$$z \approx D_{pL} ln\left(\frac{D_{pL}}{D_{pS}} \cdot \frac{E}{E_c} + 1 - \frac{D_{pL}}{D_{pS}}\right) \tag{3}$$

The following reactions describe the photopolymerization process of ECPL. When the photopolymer resin receives light energy, the photoinitiator absorbs it and decomposes into two radicals with first order rate constant K_d. Equation 4 depicts this initiation process.

$$In \xrightarrow{K_d} 2R \tag{4}$$

The radicals can then react with the double bonds to form longer chains, form a dead radical, or be quenched with dissolved oxygen, as depicted by Equations 5, 6, and 7.

$$R\cdot + DB \xrightarrow{K_p} R\cdot \tag{5}$$

$$R\cdot + R\cdot \xrightarrow{K_t} R_{dead} \tag{6}$$

$$R\cdot + O_2 \xrightarrow{K_{t,O_2}} R_{dead} \tag{7}$$

R_{dead} is the dead radical that is not able to react with monomers or polymers to form more complex chain or net structures. The rate constants used are K_p for propagation of a radical through an acrylate double bond, K_t for termination between two radicals, and $K_{t,O2}$ for termination of a radical with an oxygen molecule. The overall rate of initiator decomposition, R_i, is modeled by multiplying the rate constant K_d by the initiator concentration *[In]*, as shown in Equation 8.

$$R_i = K_d[In] \tag{8}$$

The kinetic equations for the concentrations of double bonds *[DB]*, live radicals *[R·]* and oxygen *[O_2]* is given in Equations 9, 10, and 11.

$$\frac{d[\mathrm{R}\cdot]}{dt} = 2k_d I(z)[In] - 2k_d[\mathrm{R}\cdot]^2 - k_{t,O_2}[\mathrm{R}\cdot][O_2] \tag{9}$$

$$\frac{d[DB]}{dt} = -k_p[\mathrm{R}\cdot][DB] \tag{10}$$

$$\frac{\partial[O_2]}{\partial t} = -k_{t,O_2}[\mathrm{R}\cdot][O_2] + D_{O_2}\frac{\partial^2[O_2]}{\partial z^2} \tag{11}$$

The rate constants from the ordinary differential Equations 9-11 were modeled along with a diffusion model (chdi) in COMSOL to estimate the concentration of the individual species at a given time and location within the resin chamber. The concentration of reactants, especially the monomer concentration, can be used to estimate the profile of the cured part. Carothers and Flory described a gel as an infinitely large, insoluble molecule. Flory used this definition to estimate the degree of conversion necessary for the onset of gelation based on the functionality of the reacting monomers [8]. Once the resin starts to gel, the viscosity of the solution increases sharply, and the resin undergoes a rapid transition from a liquid state to a solid state [9]. The degree of conversion is computed using Equation 12, where the initial monomer concentration is *[M_0]* and the monomer concentration after polymerization is *[M]*.

$$Conversion = \frac{[M]-[M_0]}{[M_0]} \tag{12}$$

The shape of the cured part can then be estimated by tracking the coordinates within the resin chamber where the conversion has reached the critical conversion limit. Using the aforementioned rate constants, a conversion cut-off value of 20% was determined by fitting to the experimental data for TMPTA with oxygen in [10].

2.2.2. Revision of reaction rate constants

In Jariwala et al, the rate constants, K_t, K_p, and $K_{t,O2}$ were estimated by fitting the simulation results with the experimental data from Fourier-transform infrared (FTIR) experiments [11]. However, it is suggested that the individual rate constants are not unique and may vary. Since the FTIR experiments were conducted at 100 times the intensity of the light used in the ECPL system, it is possible that the effect of oxygen inhibition and diffusion was not adequately captured using the presented rate constants. Hence, these constants were varied to suit the ECPL experimental conditions.

To investigate the effects of the rate constants on the cured height vs. time working curve, a parameter study was conducted, varying one parameter while keeping the other rates the same [12]. It was found that increasing K_p resulted in prediction of a larger cured part. $K_{t,O2}$ did not have significant influence on the working curve, and the oxygen diffusion rate had no effect on the curvature of the working curve. Thus, to revise the rate constants, the oxygen diffusion rate was found to acquire the curvature of the working curve. Then K_p was found to fit the simulation working curve to the experimental working curve, and $K_{t,O2}$ was altered to the best fit. The revised values for K_p, K_t, $K_{t,O2}$, and oxygen diffusion are 0.95 m^3/mol-s, 0.43 m^3/mol-s, 300 m^3/mol-s, and 0.42 m^2/s.

2.2.3. Numerical finite element (FE) model

Photopolymerization simulations were conducted using COMSOL software to predict the height and profile of the final cured part. The working bitmap, which has a width of 90 pixels, projects an irradiation region of 560μm. A 2D FE model was created to simulate the experimental conditions. The width of the model was taken as 1mm and the height as 200μm,

both of which match the size of the reaction chamber in the actual experimental setup. 1855 triangular elements were used in the simulation. The size of the finest mesh in the irradiation area is 8µm. Figure 6 shows the reaction chamber modeled in COMSOL. The entire rectangular reaction chamber is assumed to be filled with liquid photopolymer. All boundaries are assumed to be insulated. This closely resembles the actual experimental conditions.

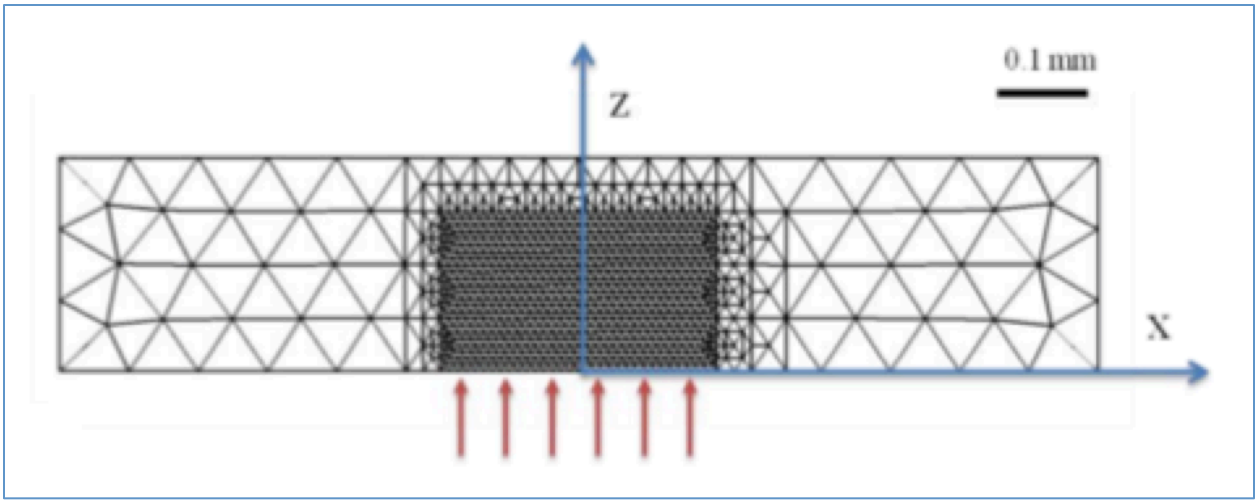

Figure 2: *Mesh model of resin chamber*

2.3 Interferometric Curing Monitoring (ICM)

The ICM system was developed to monitor the curing process by measuring the dimensions of the cured part in real time. Figure 3 shows a schematic of the system. A visible light laser is used as a source for an interferometry system based on the principles of a Mach-Zehnder interferometer. A beam expander expands the laser beam to cover the entire area of interest. The Spatial Light Modulator (SLM) system consists of an SLM chip between two polarizers and a spatial filter, which decreases the diffracted patterns. The SLM system can reduce the laser beam to a point sensor and move it in the lateral directions. The beam splitter then directs the laser beam down onto the resin chamber. The resin chamber, where the part is

cured, consists of liquid resin filled between two glass slides. The signals resulting from the combination of the reflected light are then captured by a CCD camera.

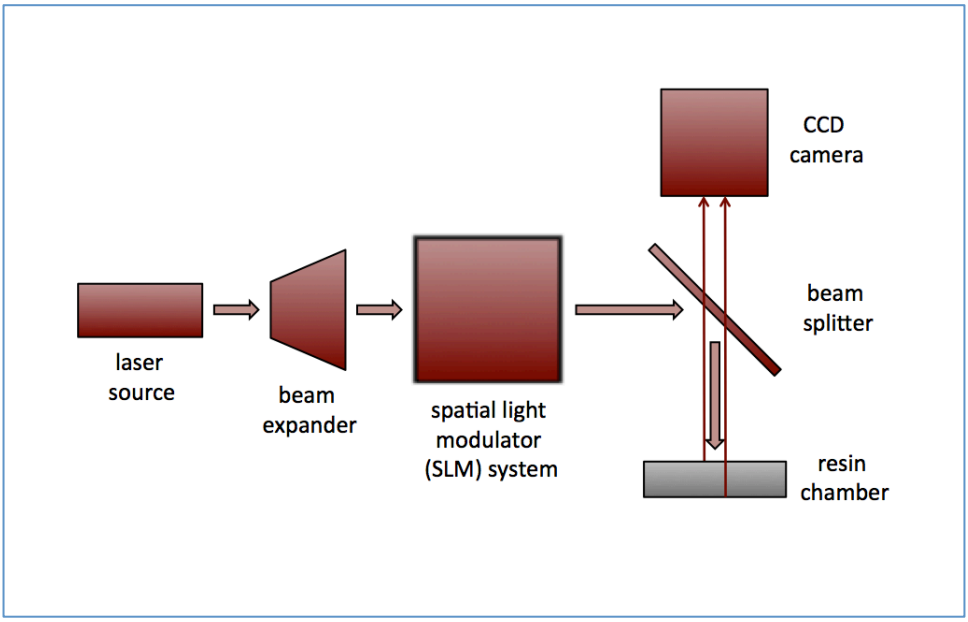

Figure 3: *Schematic of ICM system*

The ICM system detects the difference in optical path length between the light reflected from the top and bottom glass slides of the resin chamber. During the reaction, the overall refractive index of the chamber changes as part of the liquid resin is solidified. Thus, the phase of the beams reflected from the surfaces of the bottom glass slide change throughout the photopolymerization process while the phases of the beams reflected from the surfaces of the top glass slide remain constant. This generates the change in the interference patterns captured by the CCD camera.

To quantify the phase shift, the reflected light is characterized in terms of five different beams reflected from each of the interfaces of the resin chamber, as illustrated in Figure 4. The light path in Figure 4 is inclined in order to clearly illustrate the multiple reflected beams. In reality, the original beam and all the reflected beams are vertical and coincident. The recorded

signal is determined by the difference in phase between each set of two wave components depicted in the figure. All oscillating phase components are attributed to the cured height *Z*.

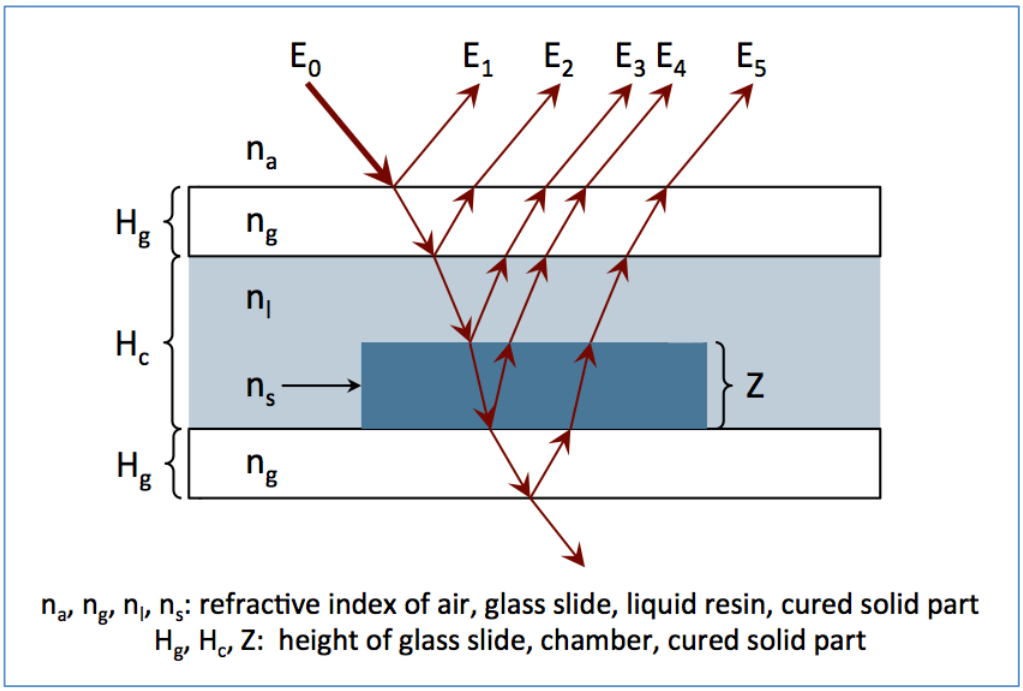

Figure 4: *Multi-beam interference optics model for ICM*

Under the assumption that all process parameters are momentarily invariant, with *Z* being the only varying factor, it becomes evident that the instantaneous frequency (IF) of the signal is dependent only upon the rate of curing, $\dot{Z}$. The aforementioned phase components comprise the four signals described in Table 1 [13]. Using experimental data from Jones et al [14], the IF values have been estimated for a part cured with an exposure intensity of about 8.86 W/m^2. The frequencies f_1 and f_2 are too high to be detected by the ICM camera, which operates with a frame rate of 30 frames/s. Therefore, the phase shift observed by the ICM system only constitutes the low frequency signal corresponding to f, which accounts for the light reflected from the top and bottom glass slides of the resin chamber. However, the presence of f_1 and f_2 could contribute to

the amplitude of the signal without affecting the phase shift. This is a possible cause of the arbitrary amplitude fluctuations in the ICM signal.

Table 1: *Instantaneous frequency analysis for ICM*

Instantaneous Frequency	Corresponding Phase	Estimated Value (Hz)
$f_0 = 0$	δ_{12}, δ_{45}	0
$f_1 = \frac{2}{\lambda} n_l \dot{Z}$	δ_{13}, δ_{23}	31.5
$f_2 = \frac{2}{\lambda} n_m \dot{Z}$	δ_{34}, δ_{35}	32.1
$f = \frac{2}{\lambda}(n_m - n_l)\dot{Z}$	$\delta_{14}, \delta_{15}, \delta_{24}, \delta_{25}$	0.6

The ICM sensor model is characterized by Equations 13 and 14, where I_M is the intensity measured by the CCD camera, I_0 is the overall average intensity, I_1 is the superposed intensity of all the interference beams with the same instantaneous frequency f, δ is the time-varying phase component in the intensity model, φ is the static superposed phase offset, n_l is the liquid refractive index, and n_m is the average refractive index of the cured solid. [13]

$$I_M = I_0 + I_1 cos\left[\frac{4\pi}{\lambda}(n_m - n_l)Z + \varphi\right] \tag{13}$$

$$2\pi f = \frac{d(\delta+\varphi)}{dt} = \frac{d\delta}{dt} = \frac{4\pi}{\lambda}(n_m - n_l) \cdot \frac{dZ}{dt} \tag{14}$$

Solving differential Equation 14 using Euler's Method yields Equation 15, where T_i is the time step of integration and f_i is the IF in the ith run of parameter estimation. [13]

$$Z = \frac{\lambda}{2(n_m - n_l)} \sum_i T_i f_i = \frac{\lambda}{2(n_m - n_l)} \cdot \varphi \tag{15}$$

In summation, for the first time period of the signal, the ICM system senses the change in the time-varying interference pattern, and estimates the IF of the interference pattern, which can then be used to estimate the height of the cured part. This procedure is repeated for each subsequent time period as the part is cured. Figure 3 shows an example of the intensity over time

graph for a point on a sample cured with a UV light intensity of 8.86 W/m^2 and exposure time of 12 s along with the total measured phase shift and estimated height [13].

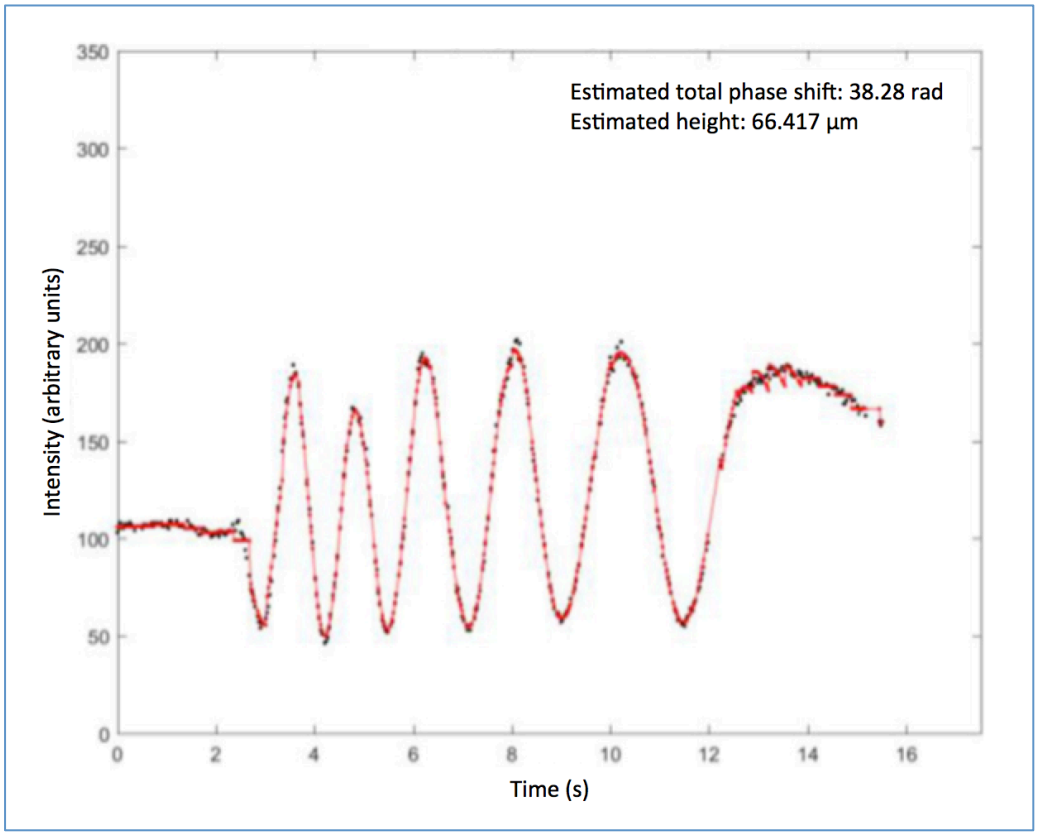

Figure 5: *Typical intensity vs. time graph*

3. RESULTS AND DISCUSSION

The process model was analyzed against experimental results, validating its ability to predict the cured part geometric profile based on the intensity and exposure time of the radiation. Additional experiments were conducted to investigate the scientific meanings of the ICM signals with the reaction kinetics of photopolymerization and verify the exactitude of the intermediate workings of the process model.

3.1 Experimental validation of process model

To test the process model, three samples were cured with exposure times of 10 s, 20 s, and 30 s, with a UV light intensity of 8.86 W/m^2. After the fabrication process, the top glass slide was removed from the resin chamber and the uncured resin was washed off using a combination of surfactant and distilled water. An Olympus LEXT OLS4100 laser confocal microscope was used to measure the cured part profile, using the bottom glass slide as the reference. Figure 6 shows the results, with the experimental cured profiles, represented by the solid lines, superimposed on the simulation predicted cured profiles, which are depicted as dashed lines. The simulation using the revised rate constants proved to be very accurate in predicting the profiles, with a dimensional error of approximately 5%.

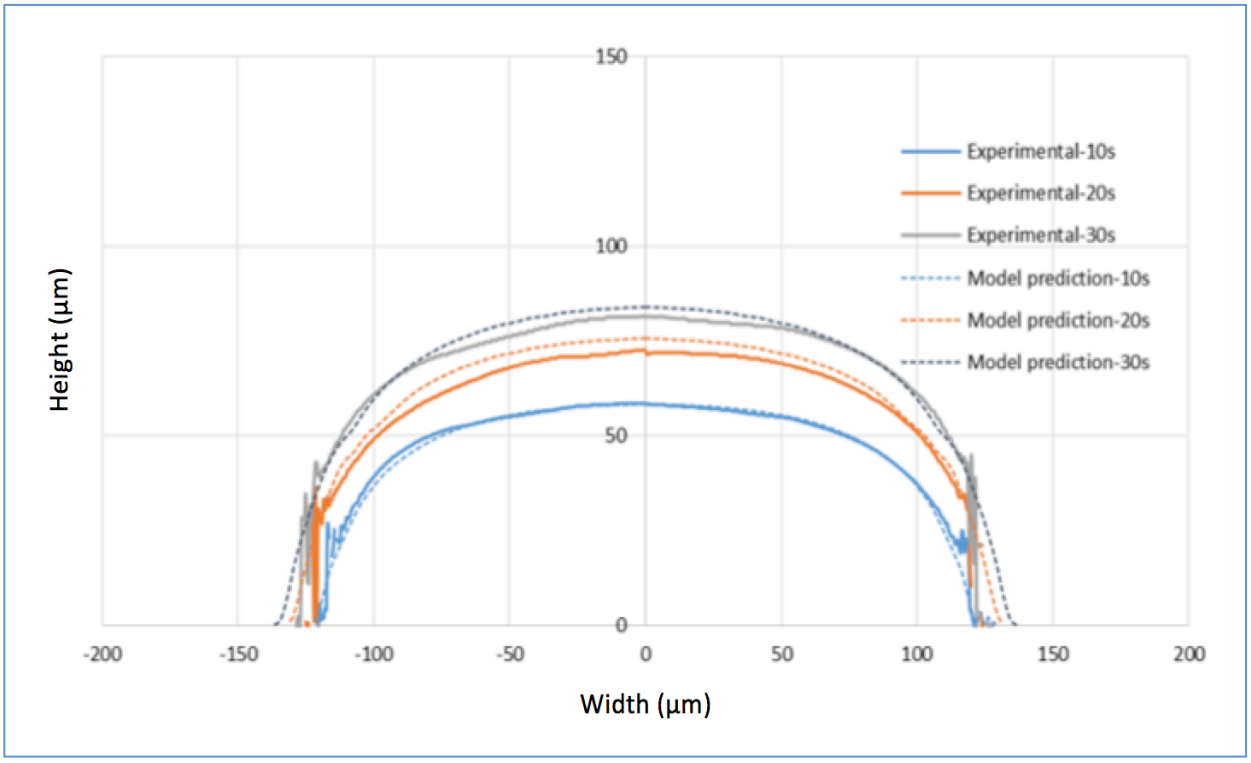

Figure 6: *Comparison of predicted and experimental cured profiles*

Figure 7 shows the simulation predicted cured height over time before and after optimization of the rate constants, where the blue line is the previous simulation prediction, the orange line is the revised simulation prediction, and the orange x's are experimental data points. It is evident that the revised rate constants result in a significantly closer match to the experimental data.

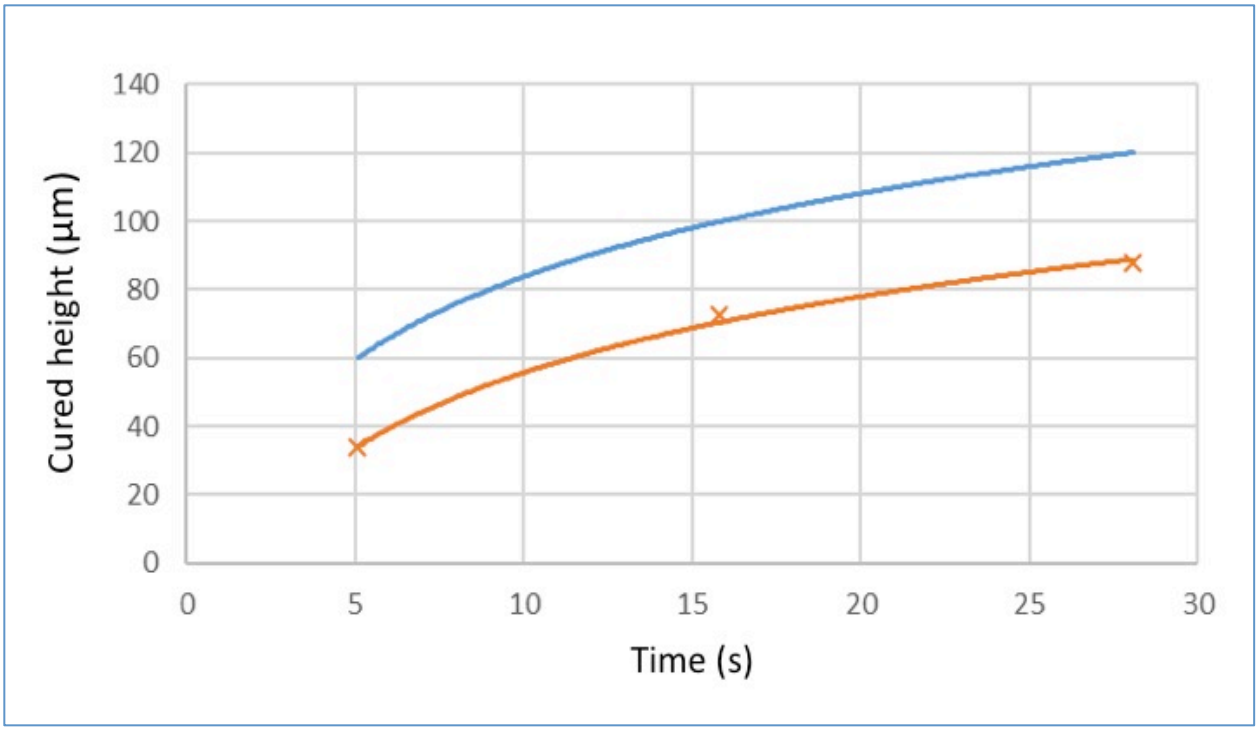

Figure 7: *Comparison of predicted height vs. time before and after rate constant revision with experimental data*

3.2. Analysis of process model with ICM

Two additional samples were cured with an exposure time of 30 s and intensities of 2.14 W/m^2 and 2.52 W/m^2, while monitored by ICM. The phase shift over time for these experiments was modeled with respect to the simulation and ICM. To calculate the phase shift from the degree of cure as predicted by the simulation, a one-dimensional vertical segment located at the center of the cured sample was considered. First, the refractive index at each second of curing was calculated. Past research confirms a linear relationship between the refractive index and the degree of conversion [15]. Using this relationship, the refractive index for each layer modeled by the simulation was calculated and then scaled based on the thickness of the layer to find the overall refractive index. Equation 16 describes this process, where Δz is the change in height

between consecutive data points, Z is the total height of the vertical range analyzed, n_s is the solid refractive index, and c_i is the degree of conversion of the ith data point.

$$n = \sum_i \frac{\Delta z}{Z}[n_s c_i + n_l(1 - c_i)] \tag{16}$$

The phase shift was then computed from the refractive index with Equation 17, where φ represents the phase shift, t is the height of the resin chamber, and λ is the wavelength of the detecting laser.

$$\varphi = 2\pi \left[\frac{2(n - n_l)t}{\lambda}\right] \tag{17}$$

Figures 9 and 10 show the results for sample 1, cured at 2.14 W/m^2, and sample 2, cured at 2.52 W/m^2. The simulation predicted results are shown in red, and the experimental phase shift over time as observed by ICM is shown in blue.

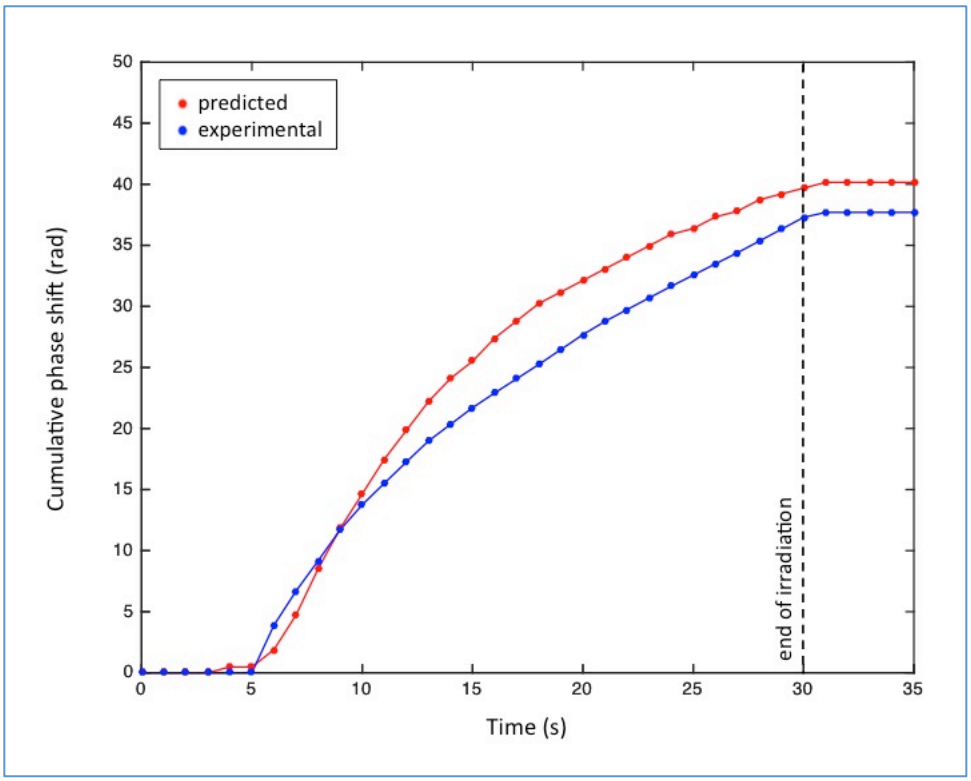

Figure 8: *Comparison of predicted and experimental phase shift over time – 2.14 W/m^2*

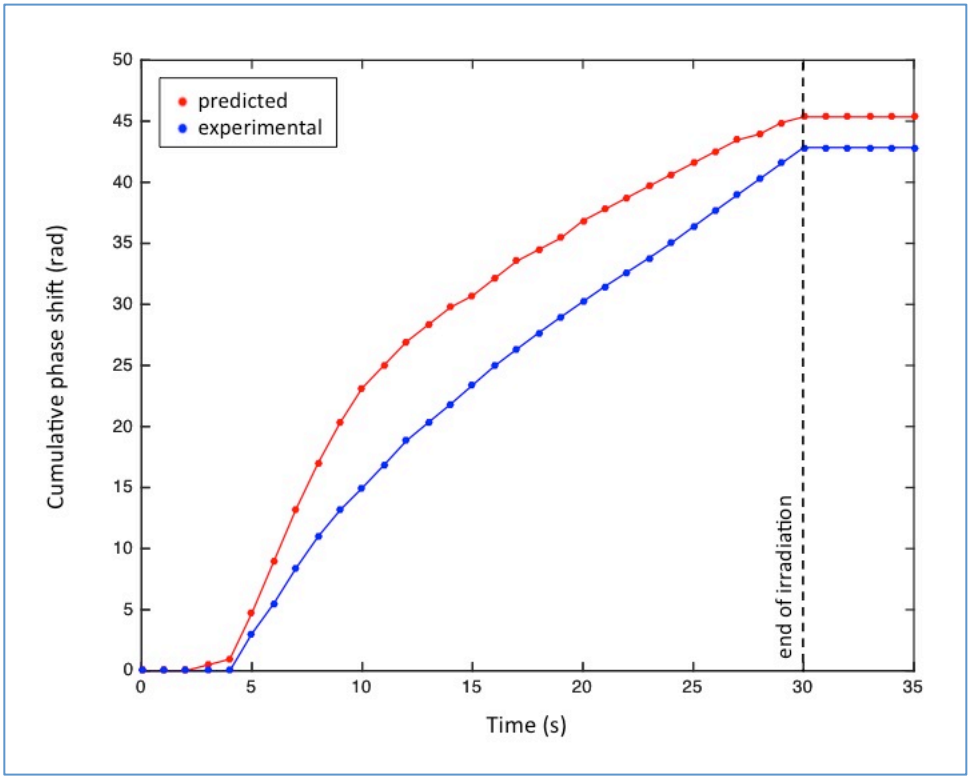

Figure 9: *Comparison of predicted and experimental phase shift over time – 2.52 W/m^2*

The similar logarithmic shape of the two distributions shows potential for the simulation to correlate with ICM. Both the simulation and ICM show the start of curing at the same time, which indicates the same amount of inhibition time. Additionally, the simulation shows no significant dark curing beyond the end of irradiation, which is consistent with the observations from ICM. However, there are a number of discrepancies that have yet to be accounted for. The simulation generally predicts slightly faster curing than is observed by ICM, and a higher total phase shift.

Considering the ICM camera frame rate of 30 frames/s, the phase shift signal captured is accurate to approximately 0.033 s. Estimating the frequency of the interference patterns for samples 1 and 2 to be 1.5 rad/s and 1.7 rad/s, respectively, yields expected errors of 0.050 rad and 0.056 rad for the ICM phase shift measurement. The COMSOL simulation has a time scale

resolution of 0.10 s. This contributes 0.15 rad and 0.17 rad to the expected errors of samples 1 and 2. Additionally, the confocal microscope measurement, which was used to calibrate the COMSOL simulation to the radiation intensity, has an error of approximately ± 1.5 μm, but this difference has a negligible effect on the simulation prediction of the degree of conversion and the subsequent phase shift calculations. Thus, the total expected errors for samples 1 and 2 are 0.20 rad and 0.22 rad. The experimental error, which amounts to 2.5 rad for both samples, does not lie within the expected error range.

There are several possible contributing factors to these disparities. Internal reflections of the laser beam within the resin chamber could alter the signals captured by the ICM camera. Additionally, the part geometry could effect how the laser light is reflected from the curing front, i.e. the light would reflect from uneven surfaces at an angle instead of directly upwards.

4. CONCLUSION

This work constitutes a comprehensive process model for mask-based stereolithography, demonstrating that the existing ECPL photopolymerization model can be improved significantly by revising the rate constants to fit experimental data. Comparing COMSOL simulated profiles for several samples with the experimental results confirms that the process model is effective in predicting the part geometry. The refractive index over time for the photopolymerization reaction was modeled based on the simulation, and the phase shift over time was subsequently determined. These results were compared to experimental ICM results, which showed a general correlation, with coincident start of curing and no significant dark reaction. The comparisons also revealed some inconsistencies between the predicted and experimental progression of curing, with the simulation predicting a larger phase shift than is shown in ICM. Future work will investigate the reasons behind the difference between phase shift over time as modeled with respect to the simulation and ICM, and aim to improve the experimental set-up to reduce these errors and/or alter the model to account for them.

REFERENCES

[1] Matyjaszewski, K. & Möller, M., 2012, *Polymer Science: A Comprehensive Reference*, Elsevier BV, Amsterdam, Chap. 4.

[2] Erdmann L., Deparnay A., Maschke G., Längle M., Bruner R., 2005, "MOEMS-Based Lithography for the Fabrication of Micro-Optical Components", *Journal of Microlithography, Microfabrication, Microsystems,* **4**(4), pp. 041601-1, -5.

[3] Mizukami Y., Rajnaik D., Rajnaik A., Nishimura M., 2002, "A Novel Microchip for Capillary Electrophoresis with Acrylic Microchannel Fabricated on Photosensor Array", *Sensors and Actuators B,* **81**, pp. 202-209.

[4] Jariwala A., Ding F., Zhao X., Rosen D., 2008, "A Film Fabrication Process on Transparent Substrate Using Mask Projection Stereolithography", D. Bourell, R. Crawford, C. Seepersad, J. Beaman, H. Marcus, eds., *Proceedings of the 19th Solid Freeform Fabrication Symposium*, Austin, Texas, pp. 216-229.

[5] Limaye, A. & Rosen, D., 2007, "Process Planning Method for Mask Projection Micro-Stereolithography," *Rapid Prototyping Journal*, **13**(2), pp. 76-84.

[6] Gibson, I, Rosen, D.W., Stucker, B., *Additive Manufacturing Technologies: Rapid Prototyping to Direct Digital Manufacturing,* Second Edition, Springer, 2015. ISBN: 978-1-4939-2113-3.

[7] Jariwala, A., Schwerzel, R., & Rosen, D., 2011, "Real-Time Interferometric Monitoring System for Exposure Controlled Projection Lithography," *Proceedings of Solid Freeform Fabrication Symposium*.

[8] Flory, P. J., "Molecular size distribution in three dimensional polymers. I. gelation," *Journal of the American Chemical Society*, **63**, pp. 3083–3090, 1941.

[9] Winter, H. H. and Chambon, F., "Analysis of linear viscoelasticity of a crosslinking polymer at the gel point," *Journal of Rheology*, **30**(2), pp. 367–382, 1986.

[10] Boddapati, A., "Modeling Cure Depth during Photopolymerization of Multifunctional Acrylates," M.S. Thesis, Georgia Institute of Technology, School of Chemical & Biomolecular Engineering, Atlanta, 2010.

[11] Jariwala A., Jones H., Kwatra A., & Rosen D. W., 2013, "Process Planning Method For Exposure Controlled Projection Lithography", *Proceedings of the 24th Solid Freeform Fabrication Symposium*, Austin, Texas, pp. 95-110.

[12] Zhang, Y., 2016, "Empirical Process Planning for Exposure Controlled Projection Lithography," M.S. thesis, School of Mechanical Engineering, Georgia Institute of Technology.

[13] Zhao, X. & Rosen, D., 2016, "Real Time Interferometric Monitoring and Measuring of Photopolymerization Based Stereolithographic Additive Manufacturing Process: Sensor Model and Algorithm," Measurement Science and Technology, **21**(1).

[14] Jones, H., Jariwala, A., and Rosen, D., 2014, "Towards Real Time Control Of Exposure Controlled Projection Lithography," *Proceedings of International Symposium on Flexible Automation*.

[15] Dorkenoo, K., van Wonderen, A., Bulou, H., Romeo, M., Crégut, O., Fort, A., "Time-resolved measurement of the refractive index for photopolymerization processes," *Applied Physics Letters*, **80**(12), pp. 2474-2476, 2003.